10TH INTERNATIONAL SYMPOSIUM ON PARTICLE IMAGE VELOCIMETRY – PIV13
Delft, The Netherlands, July 2-4, 2013

Volumetric Velocity Measurements of an Acoustic Streaming Microeddy Array using Color-Coded Three-Dimensional Micro Particle Tracking Velocimetry

W. Tien[1], D. Dabiri[1], V.H. Lieu[2], and D.T. Schwartz[2]

[1] Department of Aeronautics and Astronautics, University of Washington, Seattle, Washington, United States
whtien@uw.edu

[2] Department of Chemical Engineering, University of Washington,Seattle, Washington, United States

ABSTRACT

Steady streaming flows, also known as acoustic streaming, are the steady currents formed in a fluid undergo high frequency oscillations. Hydrodynamic tweezers is a microfluidic device utilizes this phenomenon to create the steady streaming microeddies formed by the interaction between oscillating fluid and solid boundaries that can trap objects of various sizes and densities. In this study, a microfluidic device with an array of cylinder posts built to generate the microeddy arrays was imaged by a volumetric 3-D μPTV system to investigate the flow field. The oscillation frequency is varied from 2840Hz to 20000Hz. The 3-D μPTV system utilizes a three-pinhole plate, color-coded by color filters of different wavelengths, to create a defocused exposure pattern on the image sensor plane for each particle. Since the particle image exposure is color-coded, each color channel of the color camera acts as an independent image sensor. Three independent forward scattering LED illumination sources are used to provide illumination for each color channel, and a color separation algorithm is used to minimize the measurement errors due to cross-talk between color filters. A cascade correlation peak-finding algorithm is used to resolve overlap particle images, and the particle locations are reconstructed by a calibration-based epipolar line search method. Particle tracking is done by a vision-based particle-tracking algorithm to identify, locate and track the Lagrangian motions of the tracer particles and reconstruct the flow field. The volume of imaging is 600 × 600 × 150 μm^3. The measured flow field shows that four eddies were formed around each post and dividing streamlines were formed between the posts to create a symmetric cell-like flow structure. The flow is three-dimensional and symmetric flow structure was found in the Z direction. The eddy size decreased with increasing oscillation frequency, and the eddy center moved towards the post as the frequency increased.

INTRODUCTION

Manipulation of cells and particles within a microfluidic device has been an interest in biomechanical applications [1, 2]. Compared to non-microfluidic techniques, it provides several advantages such as higher processing rate, higher spatial resolution and lower sample use. Due to the technology advances in fabrication of microfluidic devices, it becomes more cost-effective and accessible. Manipulation and trapping can be done with various mechanisms that apply force fields to control the movements of cells and particles, such as optical [3], electric [4], magnetic [5], acoustic [6] and hydrodynamic forces [7].

One of the control mechanisms is steady streaming. This is a phenomenon generated by oscillatory fluid interacting with the solid boundaries. This results in a second order steady flow pattern coming from the average stress term in the time averaged Navier-Stokes equation. The steady streaming operates at a frequency range from audible-frequency [8-11] to ultrasound [12-14]. By choosing appropriate frequencies to oscillate the flow, object of certain size can be trapped inside these eddies due to the balance of the time-averaged Lagrangian drift force to the Stokes drag force. Compare to other nonintrusive methods like optical tweezers, dielectrophoretic traps or acoustical tweezers, this technique can output a comparable magnitude of the trapping force without the need of additional an external field and operates at conditions within the physiological range for typical cells. This technique is well suited for cell separation, filtering and single cell analysis.

Marmottant and Hilgenfeldt [15] generated steady streaming by oscillating the flow around an air bubble. They showed that the bubble dynamics can be controlled to deform cell-sized lipid vesicles with much lower frequencies than acoustic streaming, in which ultrasound at MHZ level frequency is used to excite liquids directly. They also observed that the lipid vesicles followed loop-like trajectories around the bubble and accumulate at certain locations. Wang *et al.* [16] demonstrated the size-sensitive sorting of particles based on this concept. They generated the steady streaming by oscillating the bubbles attached to the side of a micro-channel. Superimposed with Poiseuille flow, they demonstrated the ability to perform size-selective particle trapping and particles releasing. In recent work, Wang *el al.* [17] investigated frequency response spectrum and oscillation modes of the bubbles. It was found that the flow patterns are

highly dependent to the oscillation frequencies and there exist device independent resonance patterns, which can be understood using an asymptotic theory approach.

Hydrodynamic tweezers, proposed by Lutz *et al.* [9], is another approach that utilizes the steady-streaming flow to trap and suspend single cells and particles. Generated by audible-frequency fluid oscillation in a micro-channel, the micro-eddies around an obstacle can capture single cells and suspend them at predictable locations. Steady streaming refers to time averaging the Navier-Stokes equations that produces average stresses that drive a steady secondary flow around obstructions. Adjacent to the circular cylinder inside the micro-channel, four steady eddies can be formed symmetrically. To demonstrate the feasibility of the concept, a motile phytoplankton (Prorocentrum micans cell) is put to the micro-channel filled with sea water, and the cell is successfully trapped and released by changing the oscillation amplitude and frequency. Experimental results show that trapping forces up to 30pN are generated while exerting moderate shear stresses ($\leq$1.5N/m^2) on the trapped cell.

Although the technique has been proved to be highly feasible, the physics behind it is still not fully understood. Lutz *et al.* [8] performed a flow visualization experiment with a scale-up model to image the steady streaming behavior near a single cylinder in an oscillating flow inside a rectangular channel. The flow behavior is characterized by several parameters: the channel height h, the diameter of the cylinder a, the Stokes layer thickness δ_{AC}, which is related to the oscillating flow, and the boundary layer thickness δ_{DC}, which is related to the near-cylinder eddy size. Chong *el al.* [17] performed a theoretical and numerical analysis to investigate the motion of an inertial particle in a streaming flow created by a circular cylinder of Reynolds number order 10. In the simulation, they showed the particle followed an inward-spiral trajectory and trapped inside of the steady eddies. They showed that it is the Faxen correction terms that divert the particles from the fluid particle trajectories, while the Saffman lift force contributes most of the trapping motion.

The current theories treat the steady streaming flows as a 2-D flow, but the flow visualization work by Lutz *et al.* [8] also reveals interesting 3-D flow structures. They found that when δ_{AC}/h is small, the flow in the core region of the channel is not affected by the wall effect and the flow behavior can be simulated by 2D steady streaming around a cylinder in an unbounded flow. However, outside the core region, the flow is 3-D and strongly affected by the wall. Lieu *et al.* [11] tested this technique with arrays of cylinders in the micro-channel and found that steady streaming form a cellular pattern in the channel and agree with the 2-D simulation results in the core region. Wall protrusion and cavity were also proved to be able to trap particles or cells, but the latter with much weaker trapping force.

Due to the limitation of the visualization technique, these previous studies are focused on the flow patterns observed by a 2-D slice of the flow, or the streak lines formed by long exposures of the particle images. As shown in the 2-D flow visualization results in Lutz *et al.* [8], the flow is three-dimensional but only confined in a thin layer, but it is a scaled-up model and is made of rigid material. The question is whether the flow shows the same characteristics under the small scale model made of compliant material. To answer this question, a volumetric velocimetry technique is required to reveal the three-dimensional steady streaming flow pattern.

Microscale volumetric velocimetry is a branch of the 3-D velocimetry and is getting more and more attention due to the increasing demands to measure the flow fields for microfluidic applications. The high magnification and small image volume pose quite different technical challenges than the macro-scale counter-part. Various approaches were proposed during the last decades. The multiple-camera approaches, including Stereoscopic technique [18-20] and Tomographic PIV/PTV [21] are a direct miniaturization of the macro-scale techniques; with multiple views from different angles, the out-of-plane velocity components can be reconstructed. Due to the complexity of the optical setup and requirements of a specialized microscope, more preparation is needed to prepare and perform an experiment.

Single camera volumetric velocimetry techniques utilize various ways to reconstruct the out-of-plane velocity components. Scanning confocal µPTV [22, 23] scans through the entire image volume with a spinning pinhole array disk to allow the confocal microscope to focus at different depth locations. The dynamic range of measured velocities and measurable image depth are the main limiting factors of this technique. Digital holographic microscopy [24-28] reconstructs the whole image volume using recorded hologram. While the reconstruction can be accurate and the setup is quite simple for micro-scale applications, the hologram reconstruction algorithm is very computationally intensive and time consuming. Other techniques rely on the relation between the depth locations to the changes of defocused particle image to determine the particle location. Wave-Front Sensing/ Astigmatism Particle Tracking Velocimetry (APTV) [29-32] utilizes an additional cylindrical lens other than the field lens to create an anamorphic imaging system. The particle images thus deform differently in the x and y direction when the particle is out of focus, so the lengths of the x and y axes of the elliptical particle image relates to the depth location of the particle uniquely. The main advantage of this technique is the ease of changing the size of the measuring depth range by either changing the different focal length of the cylindrical lens or the distance between the cylindrical lens and the spherical lens. Some defocusing techniques calculate the particle depth location based on the diffraction ring patterns of the particle image [33-37]. The depth location can be determined with high resolution and no additional optics is required to perform the measurement. However, due to the complex diffraction ring structure to calculate the depth location, the particle image density needs to be kept low in order to accurately identify individual particles.

The last category of the micro-scale volumetric velocimetry technique uses multiple pinholes to create multiple exposures of the same particle on the image plane to create certain patterns. The particle location can be calculated by

relating the pattern size variation related to the depth location. This concept was first proposed by Willert and Gharib [38] and adapted to micro-scale applications [39-42]. The main advantage of this technique is the potential to have a better balance between computational cost and particle density.

In this work a 3-D µPTV technique, based on the multiple pinhole approach [42, 43], is applied to measure the 3-D flow around the hydrodynamic tweezers to investigate the flow phenomenon. The modification in this technique can capture higher particle image densities and a large measurable depth to image ratio, simply by imaging the whole micro-channel with a single camera view. A post array microfluidic device from Lieu *at al.* [44] was tested at different frequencies to show the frequency dependent flow patterns.

EXPERIMENT METHODS

Micro-channel Setup

In the current study, the micro-channel used was made of PDMS (Polydimethylsiloxane) using softlitography [45, 46]. The PDMS channel was molded from a master of epoxy-based negative photoresist (SU-8) and plasma bounded to a drilled coverslip on one side and a glass slide on the other side, as shown in Figure 1 (a). The SU-8 master was made by contact lithography and the details can be found in Lieu *et al.* [11]. The drilled coverslip provides access to load the fluid and tracer particles. Two single layer piezoelectric disks were attached on top of the coverslip, right above the cavities in the micro-channel, as shown in Figure 1 (c). The piezoelectric disks were connected to an audio amplifier and a function generator. The function generator generated a sinusoidal voltage signal at audio frequency (1 KHz – 20 KHz), amplified by the audio amplifier and drove the piezoelectric disk to vibrates at a displacement amplitudes of 1-3 µm. The vibration was transferred into the cavities in the micro-channel and created the oscillating flow required to produce the steady streaming flow.

The micro-channel is 120µm high and 1000µm wide, and a length of 30mm. The cylinder posts were in the middle of the channel and formed an array pattern. The post size and pattern varies for each testing case. The sizes of cylinder posts were 50 µm in diameter (Please refer to Figure 1 (b)). For the array pattern, the spacing between the posts is 120 µm. 1µm polystyrene particles (Fluoresbrite® Multifluorescent Microspheres) were used as tracer particles (ρ_p = 1.05 g/cm3) in water for the current study. The Stokes number defined as

$$St = 2{d_p}^2 \rho_p \omega / 9\mu, \tag{1}$$

where ω is the frequency of the oscillation, and μ is the fluid dynamic viscosity. The calculated Stokes number is 0.00012 ~ 0.0023 at the audio frequency range and is negligible.

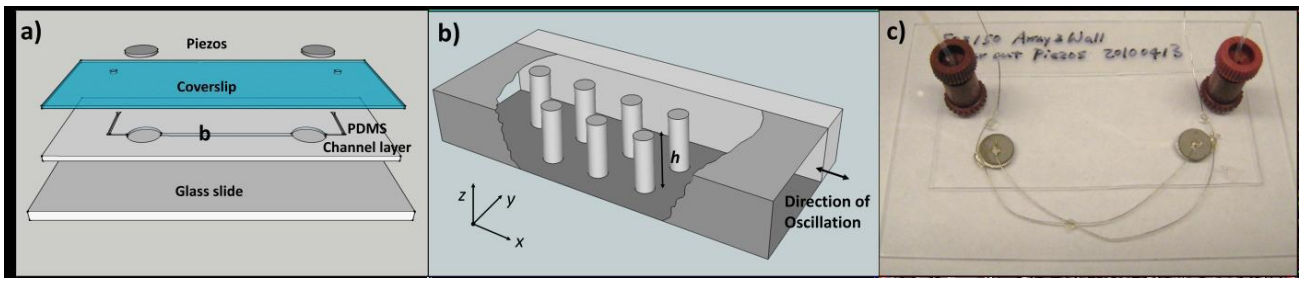

Figure 1 Setup of the trapping micro-channel with micro cylinder array. From Lieu *et al.* [11]

3-D µPTV System

The 3-D µPTV System developed by Tien *el al.* [43] allows for higher particle image density without sacrificing the measurable image depth. The main concept is to utilize color-coded pinholes to reduce the ambiguity problem of matching the triplets from a monochrome image and raise the achievable particle image density by a factor of three. A color separation scheme based on principle component transformation (PCT) is used to separate the different color exposures from the raw color image into individual pinhole images. The detail of the algorithm is described in [42]. In each pinhole image, the location of the particle exposure image is calculated by approximating it using a Gaussian intensity profile and the possible particle image overlap is resolved using a modified Cascade Correlation Method (CCM) described in Lei *el al.*[47] .

Once the location of the particle image exposures at each pinhole plane is calculated, the triplet is identified by an epipolar line search method similar to [48]. The particle location is then calculated by a calibration-based method described in Tien *et al.*[42]. A set of calibration images of known particle locations are taken by moving a dot-pattern

target plate with a high precision translation stage (APT 600, Thorlabs). A glass slide spin-coated with a PDMS layer of the same thickness to the device was used for calibration to match the index of refraction. The mapping functions between each exposure image coordinates and the spatial location of the calibration dots are built with radial base functions (RBF) written in a MATLAB routine by Chirokov [49]. In the actual experiment, the Z coordinate of the particle spatial coordinate is first found by the mapping functions between the exposure locations of each pinhole image. The X and Y coordinates of the particle location are then calculated by the mapping function built from the calibration. Two of the three exposure locations are necessary to calculate the spatial coordinates of the particle, but all three pinhole pairs (red to green, green to blue and blue to red) are used to get the coordinates, and the average values are used to improve the accuracy. The mean error of the depth location measurement is less than 1.5% of the full measurable depth range, and the uncertainty is less than 0.05% for the in-plane directions (X and Y) and 0.25% for the depth location (Z). Both the mean and standard deviation of the errors are lower than 1% of the full measurement range, which are on the same level with the location error. For more details of the technique, interested readers may refer to Tien *el al.*[42].

After particle locations are found, particle tracking is used to resolve the velocity field. A particle tracking algorithm adapted from a method used in computer vision [50] is used. The implementation of the method is hybridized with PIV results, and an iterative scheme with outlier detection method by Duncan *el al.* [51] is used to increase its robustness to deal with the out-of-volume particles. The algorithm is described in our previous work [47](Lei et al. 2012), and an extension from 2-D to 3-D is used in the current work. The guiding 3-D PIV field is built using a 3-D cross-correlation method developed by Pereira *el al.*[52].

The experimental setup of the 3-D µPTV system is shown in Figure 2 (a). Three Cree XR-E series LEDs with Red (620 nm), Green (520nm) and Royal Blue (460 nm) are used to provide a continuous light source. Each LED is aligned with a lens doublet to focus the light to the object plane. Because the light is from an inclined angle aligned with the corresponding pinhole, the scattering angle of the light to the other two pinholes are significantly away from the optimized scattering angle (≈ 0°). Therefore only the wavelength of light coming from the matched light source results in the particle image exposure for the corresponding pinhole, and the peak shift due to color aberration can be minimized. A 3-pinhole plate is placed in the objective lens ((Olympus UPLanFLN 10X) right after the lens elements, as shown in Figure 2 (b). The pinhole plate pattern is shown in Figure 2 (c). The diameter of each pinhole is d = 2.53 mm, and the distance R (from the pattern center to each pinhole center) is 3 mm, results in a pinhole separation distance of 5.196mm. Each pinhole is attached with a color filter (Lee 781 Terry Red, Lee 738 JAS Green and Lee 798 Crysalis Pink) to allow only certain range of light wavelength to pass through each pinhole. This configuration results in an imaging volume of 600 ×600×240 µm.

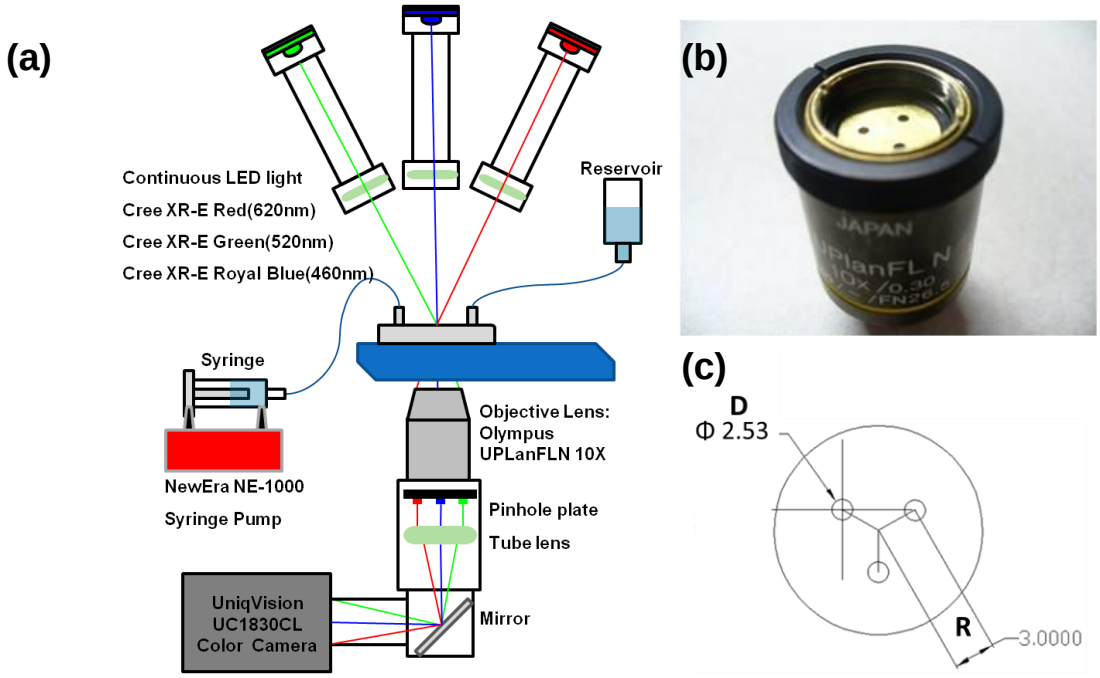

Figure 2 Experimental Setup of the 3-D µPTV system: (a) Schematic of the experimental setup (b) Pinhole plate inserted in the microscope objective lens (c) drawing of the pinhole plate dimension

A 1024 pixel × 1024 pixel resolution color CCD camera (uniqvision UC-1830CL) with a frame rate of 30 frame per second is used to capture images. The typical exposure time is set to 4.167 ms (1/240 s). The data rate is 15 Hz. Images are captured and recorded by software (Video Savant® 4, IO Industries Inc.) through a frame grabber board

(Road Runner R3 CL, Bitflow Inc.) into a PC. For each case, 180 image pairs are processed and an average of 982 vectors is found for each image pair. The PTV vector fields are scattered data and the spacing is not uniform, so an interpolation back to uniform grid is necessary in order to further analyze the data. For steady streaming, the averaged velocity component is of main interest, therefore the PTV fields are combined together and interpolated by an inverse-distance weighting scheme to resolve the steady streaming flow. The interpolated grid size is 10 ×10 × 10 μm. In all results shown, the oscillation is in the X direction.

RESULTS AND DISCUSSION

Figure 3 shows the reconstructed 3-D flow field of an in-line array post configuration at an oscillation frequency of 2840Hz. The main feature observed is that the flow formed a cell-like structure around each post. Because of the tight spacing, the eddies were confined to the cell and dividing streamlines are formed in between each cell. The flow patterns were also more three dimensional.

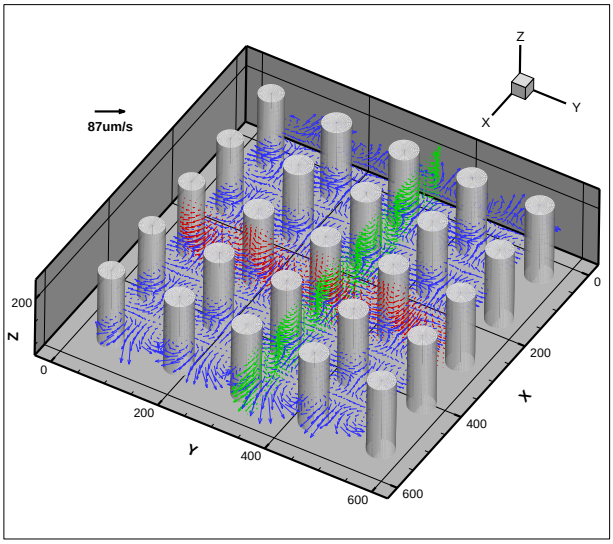

Figure 3 Reconstructed 3-D Flow field of in-line array configuration at 2840Hz. Only a slice of vector field for each X-Y, Y-Z and X-Z plane is shown

Slices of the flow field at *Y*-*Z* plane of the in-line array post configuration are shown in Figure 4. The *X* locations of the cross-section are chosen to show the variation of the flow field around a single post in the array. The *X* vorticity map is also shown in each figure, and the out-of-plane velocity vector (the *X* component) is shown in grayscale to help to demonstrate the 3-D flow pattern. The flow at the post center cross-section (*X*=50, Figure 4 (a)) shows that the flow was symmetric across the *Z* direction, and the flow direction was away from the post. The flows from the adjacent post meet together and formed a dividing streamline in the middle of the two posts. The vorticity map shows 4 major vorticity concentrated regions and they were located at the four corners in between the two adjacent posts. As *X* increases, the flow direction turned around between *X*=70 (Figure 4 (b)) and *X*=90 (Figure 4 (c)). This turning also resulted in a change sign of the *X* vorticity and formed an inversed vorticity pattern. Although without the posts, at *X*=110 and 130 (Figure 4 (d) and (e)), the flow pattern was still aligned well with the post, forming the dividing stream plane aligned with the center of the post.

Slices of the flow field at *X*-*Z* plane of the in-line array post configuration are shown in Figure 5. Similar to the *Y*-*Z* planes, the *X*-*Z* planes are selected to show the flow variations inside the cell and vorticity map is overlaid with the vector plot. At *Y*=210 (Figure 5 (e)), the flow direction was towards the post from the dividing stream plane in the middle of the two post (the 2nd post is not shown in the scaled up picture). As *Y* decreased, the flow turned around between *Y* =195 (Figure 5 (d)) and *Y*=180 (Figure 5 (c)). At *Y*=165 (Figure 5 (b)) and *Y*=150 (Figure 5 (a)), four vorticity concentrated regions were formed and the dividing stream plane was formed at the *X* location of the post.

Figure 6 shows the 2-D velocity field at 4 different frequencies (2840, 5800, 11360 and 20000Hz) of the in-line array post configuration, overlaid with the *Z* component of the vorticity contour and the W component of velocity are shown in gray scale together with the velocity vectors of U and V components. With the increase of frequency, the eddy size around each post decreases, and the center of the eddy is moving towards the post. At 20000 Hz (Figure 6(d)), the eddy flows were mostly concentrated near the post and the boundaries of the flow cell become weak compared to the low frequency cases.

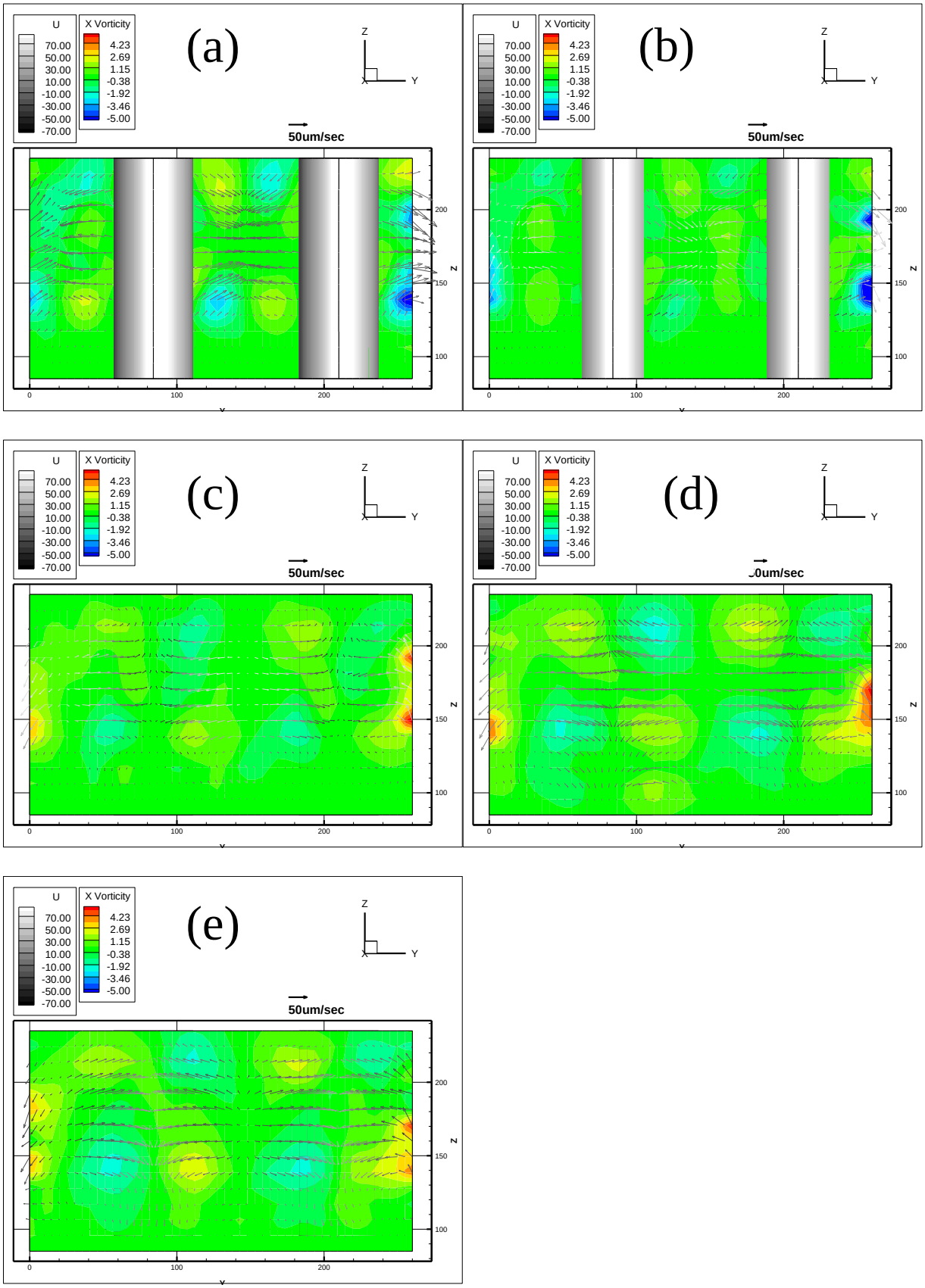

Figure 4 Partial Velocity Profile at Y-Z plane of the in-line array post configuration at (a) X= 50, (b) 70, (c) 90, (d) 110 and (e) 130. U component is shown by the gray scale and the X vorticity is shown by contour plot on the background

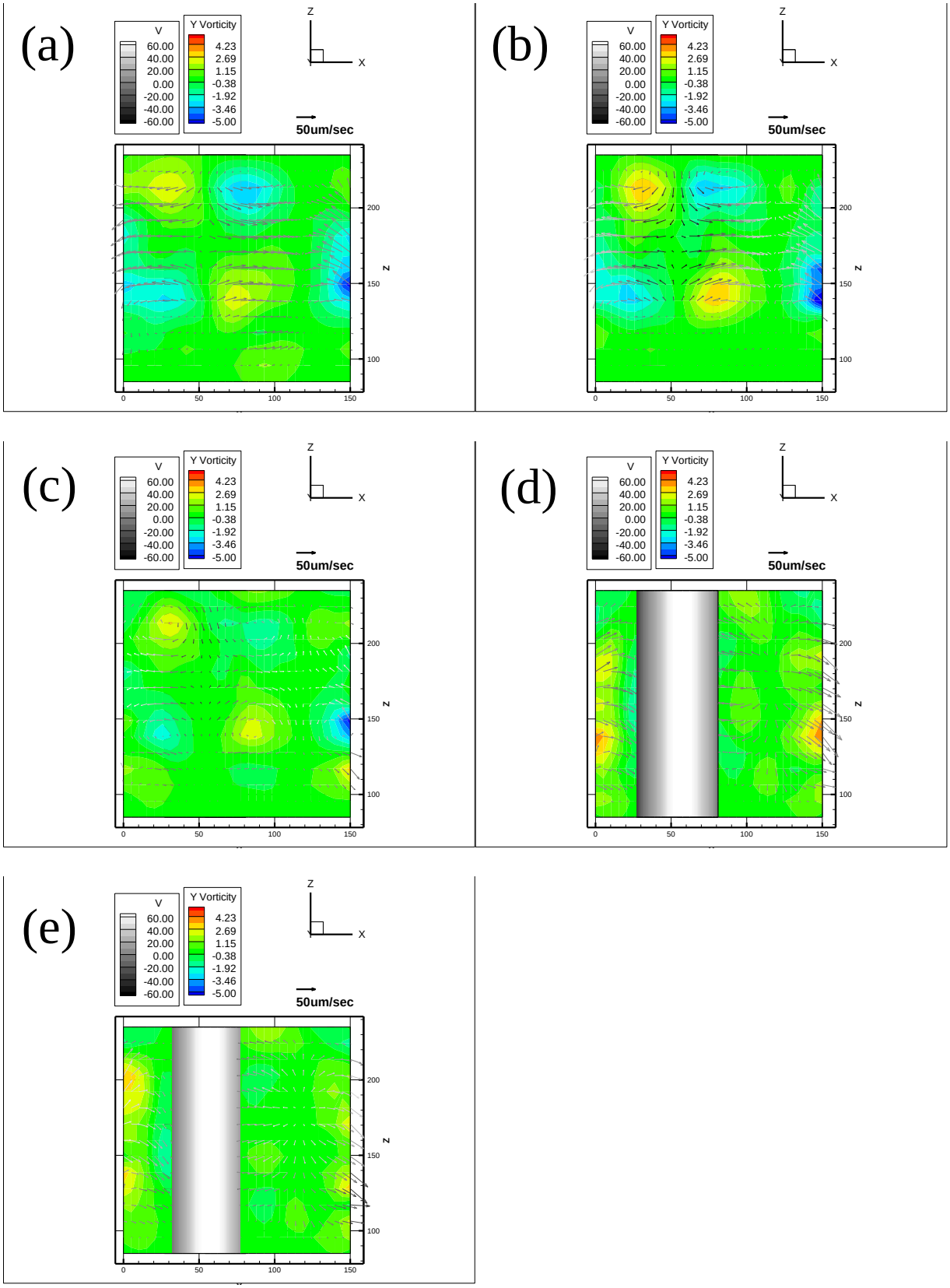

Figure 5 Partial Velocity Profile at X-Z plane of the in-line array post configuration at (a) Y= 150, (b) 165, (c) 180, (d) 195 and (e) 210. V component is shown by the gray scale and the Y vorticity is shown by contour plot on the background

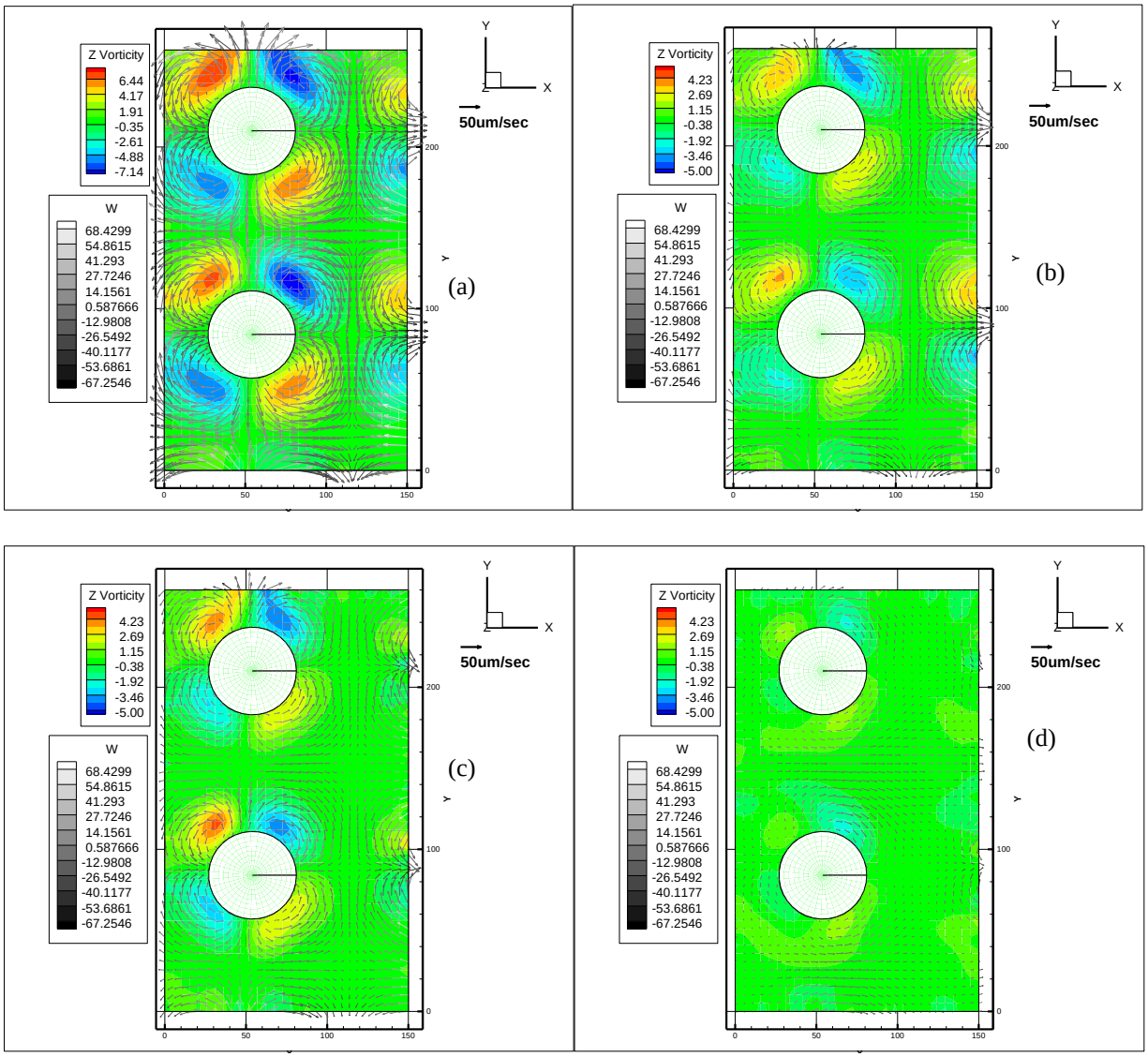

Figure 6 Partial Velocity Profile at X-Y plane of the in-line array post configuration at Z= 160 and oscillation frequency at (a) 2840, (b) 5800, (c) 11360 and (d) 20000 Hz. W component is shown by the gray scale and the Z vorticity is shown by contour plot on the background

In all different frequencies, the measured flow field showed three dimensional flow structures, with four eddies observed around each post. Lutz *et al.* [8] showed that steady streaming eddies formed by a cylinder post can be characterized by the DC boundary layer thickness δ_{DC}. When δ_{DC} is small or comparable to the cylinder radius, a counter-rotating induced eddy structure will present. 2-D analytical solution showed that the normalized eddy size δ_{DC} /*a* can be related to the normalized Stoke Layer thickness for the cylinder δ_{AC} /*a*, where *a* is the radius of the cylinder post, and $\delta_{AC} = \sqrt{\nu/\omega}$, where ν is the kinematic viscosity and ω is the oscillation frequency. The analytic curve is confirmed by their experimental results ([8], fig. 5). The current work uses water ($\nu = 0.0095 cm^2/s$) as the medium, with a frequency from 2840 Hz to 20000 Hz. The post size is 25 μm in radius and the calculated δ_{AC} /*a* = 0.29 ~ 0.11. The values are from outside the right end to the middle range of the curve, which means that δ_{DC} range from much larger than *a* to comparable to the size of the cell and explains why in the results only the steady streaming eddies were present.

In the same study, Lutz *et al.* [8] also related the Stoke layer thickness δ_{AC} /*h* to the DC boundary layer thickness for junction streaming Δ_{DC}/*h*, which was defined as twice the distance of the center of the junction streaming eddy from channel wall. The junction streaming eddy is formed outside the 2-D steady streaming eddies, and limits the thickness of the 2-D eddies. They found that Δ_{DC}/*h* is roughly proportional to δ_{AC} /*h* ([8]). In the current work δ_{AC} /*h* = 0.10 ~ 0.04, which is from outside to the middle of the curve. This indicates that Δ_{DC} ranges from comparable to h to roughly a quarter of the height of channel and the 3-D layer is not negligible. This estimation is in agreement with the results shown in the previous section, which shows the flow fields are three-dimensional.

The basic flow pattern in the current channel shows highly symmetric cell-like structure. The flow is symmetric in *X, Y* and *Z* directions, and the 4 eddies had the same size and shape. The dividing stream plane formed by the adjacent eddies defined the flow regime of each eddy. These eddies should extend longer but were interfered with other eddies caused by the adjacent posts, therefore formed the array structure. This is the most preferable design for the hydrodynamic tweezers application, since the flow pattern of this configuration is very symmetric, it can be expected that the trapping performance of each post should be very similar. The change in frequency alters the flow structure and reduces the eddy size. This is also in agreement with the results shown in Lieu *el al.*[11], which the distance between the center of the eddy and the post surface is found to be linearly related to the Stoke Layer thickness.

CONCLUSION

Using the 3-D μPTV system, the three-dimensional flow structure of a hydrodynamic tweezers was successfully measured for the first time. For the in-line circular post array configuration, the steady streaming flow structure is found to be three-dimensional and formed a cell-like structure between the posts. Four symmetric eddies were found around each post and the flow cell was divided by the dividing streamline formed by these eddies. Increasing the oscillation frequency caused the eddy size to decrease, and the eddy center was also found to be closer to the post surface.

REFERENCES

[1] Nilsson, J., Evander, M., Hammarstrom, B., 2009, "Review of Cell and Particle Trapping in Microfluidic Systems," Analytica Chimica Acta, **649**(2) pp. 141-157.

[2] Karimi, A., Yazdi, S., and Ardekani, A., 2013, "Hydrodynamic Mechanisms of Cell and Particle Trapping in Microfluidics," Biomicrofluidics, **7**pp. 021501.

[3] Yang, A. H., Moore, S. D., Schmidt, B. S., 2009, "Optical Manipulation of Nanoparticles and Biomolecules in Sub-Wavelength Slot Waveguides," Nature, **457**(7225) pp. 71-75.

[4] Cohen, A. E., 2005, "Control of Nanoparticles with Arbitrary Two-Dimensional Force Fields," Physical Review Letters, **94**(11) pp. 118102.

[5] Lee, H., Purdon, A., and Westervelt, R., 2004, "Manipulation of Biological Cells using a Microelectromagnet Matrix," Applied Physics Letters, **85**(6) pp. 1063-1065.

[6] Evander, M., Johansson, L., Lilliehorn, T., 2007, "Noninvasive Acoustic Cell Trapping in a Microfluidic Perfusion System for Online Bioassays," Analytical Chemistry, **79**(7) pp. 2984-2991.

[7] Dylla-Spears, R., Townsend, J. E., Jen-Jacobson, L., 2010, "Single-Molecule Sequence Detection Via Microfluidic Planar Extensional Flow at a Stagnation Point," Lab on a Chip, **10**(12) pp. 1543-1549.

[8] Lutz, B. R., Chen, J., and Schwartz, D. T., 2005, "Microscopic Steady Streaming Eddies Created Around Short Cylinders in a Channel: Flow Visualization and Stokes Layer Scaling," Physics of Fluids, **17**(2) pp. 023601.

[9] Lutz, B. R., Chen, J., and Schwartz, D. T., 2006, "Hydrodynamic Tweezers: 1. Noncontact Trapping of Single Cells using Steady Streaming Microeddies," Analytical Chemistry, **78**(15) pp. 5429-5435.

[10] Lutz, B. R., Chen, J., and Schwartz, D. T., 2006, "Characterizing Homogeneous Chemistry using Well-Mixed Microeddies," Analytical Chemistry, **78**(5) pp. 1606-1612.

[11] Lieu, V. H., House, T. A., Crawford, J. T., 2011, "Microeddy design and application for single cell trapping and monitoring," Solid-State Sensors, Actuators and Microsystems Conference (TRANSDUCERS), 2011 16th International, pp. 286-289.

[12] Marmottant, P., and Hilgenfeldt, S., 2004, "A Bubble-Driven Microfluidic Transport Element for Bioengineering," Proceedings of the National Academy of Sciences of the United States of America, **101**(26) pp. 9523-9527.

[13] Wang, C., Jalikop, S. V., and Hilgenfeldt, S., 2011, "Size-Sensitive Sorting of Microparticles through Control of Flow Geometry," Applied Physics Letters, **99**(3) pp. 034101-034101-3.

[14] Wang, C., Jalikop, S. V., and Hilgenfeldt, S., 2012, "Efficient Manipulation of Microparticles in Bubble Streaming Flows," Biomicrofluidics, **6**pp. 012801.

[15] Marmottant, P., and Hilgenfeldt, S., 2003, "Controlled Vesicle Deformation and Lysis by Single Oscillating Bubbles," Nature, **423**(6936) pp. 153-156.

[16] Wang, C., Jalikop, S. V., and Hilgenfeldt, S., 2011, "Size-Sensitive Sorting of Microparticles through Control of Flow Geometry," Applied Physics Letters, **99**(3) pp. 034101-034101-3.

[17] Chong, K., Kelly, S. D., Smith, S., 2013, "Inertial Particle Trapping in Viscous Streaming," Physics of Fluids, **25**pp. 033602.

[18] Lindken, R., Westerweel, J., and Wieneke, B., 2006, "Stereoscopic Micro Particle Image Velocimetry," Experiments in Fluids, **41**(2) pp. 161-171.

[19] Bown, M. R., MacInnes, J. M., Allen, R. W. K., 2006, "Three-Dimensional, Three-Component Velocity Measurements using Stereoscopic Micro-PIV and PTV," Measurement Science & Technology, **17**(8) pp. 2175-2185.

[20] Yu, C., Yoon, J., and Kim, H., 2009, "Development and Validation of Stereoscopic Micro-PTV using Match Probability," Journal of Mechanical Science and Technology, **23**(3) pp. 845-855.

[21] Kim, H., Westerweel, J., and Elsinga, G. E., 2013, "Comparison of Tomo-PIV and 3D-PTV for Microfluidic Flows," Measurement Science and Technology, **24**(2) pp. 024007.

[22] Park, J. S., and Kihm, K. D., 2006, "Use of Confocal Laser Scanning Microscopy (CLSM) for Depthwise Resolved Microscale-Particle Image Velocimetry (Mu-PIV)," Optics and Lasers in Engineering, **44**(3-4) pp. 208-223.

[23] Klein, S., Moran, J., Frakes, D., 2012, "Three-Dimensional Three-Component Particle Velocimetry for Microscale Flows using Volumetric Scanning," Measurement Science and Technology, **23**(8) pp. 085304.

[24] Satake, S., Kunugi, T., Sato, K., 2006, "Measurements of 3D Flow in a Micro-Pipe Via Micro Digital Holographic Particle Tracking Velocimetry," Measurement Science & Technology, **17**(7) pp. 1647-1651.

[25] Satake, S., Kunugi, T., Sato, K., 2005, "Three-Dimensional Flow Tracking in a Micro Channel with High Time Resolution using Micro Digital-Holographic Particle-Tracking Velocimetry," Optical Review, **12**(6) pp. 442-444.

[26] Sheng, J., Malkiel, E., and Katz, J., 2006, "Digital Holographic Microscope for Measuring Three-Dimensional Particle Distributions and Motions," Applied Optics, **45**(16) pp. 3893-3901.

[27] Ooms, T. A., Lindken, R., and Westerweel, J., 2009, "Digital Holographic Microscopy Applied to Measurement of a Flow in a T-Shaped Micromixer," Experiments in Fluids, **47**(6) pp. 941-955.

[28] Choi, Y., and Lee, S., 2009, "Three-Dimensional Volumetric Measurement of Red Blood Cell Motion using Digital Holographic Microscopy," Applied Optics, **48**(16) pp. 2983-2990.

[29] Angarita-Jaimes, N., McGhee, E., Chennaoui, M., 2006, "Wavefront Sensing for Single View Three-Component Three-Dimensional Flow Velocimetry," Experiments in Fluids, **41**(6) pp. 881-891.

[30] Towers, C. E., Towers, D. P., Campbell, H. I., 2006, "Three-Dimensional Particle Imaging by Wavefront Sensing," Optics Letters, **31**(9) pp. 1220-1222.

[31] Cierpka, C., Segura, R., Hain, R., 2010, "A Simple Single Camera 3C3D Velocity Measurement Technique without Errors due to Depth of Correlation and Spatial Averaging for Microfluidics," Measurement Science & Technology, **21**(4) pp. 045401.

[32] Cierpka, C., Rossi, M., Segura, R., 2011, "On the Calibration of Astigmatism Particle Tracking Velocimetry for Microflows," Measurement Science & Technology, **22**(1) pp. 015401.

[33] Mendoza, M. D., 2000, "Particle Positioning from a Single CCD Image for Application to Velocimetry: Theory and Comparison to Experiment," Appl.Opt., **39**(28) pp. 5117.

[34] Guerrero J A, Mendoza-Santoyo F, Moreno D, Funes-Gallanzi M and Fernandez,S., 2000, "Particle Positioning from CCD Images: Experiments and Comparison to the Generalized Lorenz-Mie Theory," Meas.Sci.Technol., **11**(5) pp. 568.

[35] Zhang, Z., and Menq, C., 2008, "Three-Dimensional Particle Tracking with Subnanometer Resolution using Off-Focus Images," Applied Optics, **47**(13) pp. 2361-2370.

[36] Park, J. S., and Kihm, K. D., 2006, "Three-Dimensional Micro-PTV using Deconvolution Microscopy," Experiments in Fluids, **40**(3) pp. 491-499.

[37] Peterson, S. D., Chuang, H., and Wereley, S. T., 2008, "Three-Dimensional Particle Tracking using Micro-Particle Image Velocimetry Hardware," Measurement Science & Technology, **19**(11) pp. 115406.

[38] Willert C E and Gharib,M., 1992, "Three-Dimensional Particle Imaging with a Single Camera," Exp.Fluids, **12**(6) pp. 353.

[39] Yoon, S. Y., and Kim, K. C., 2006, "3D Particle Position and 3D Velocity Field Measurement in a Microvolume Via the Defocusing Concept," Measurement Science & Technology, **17**(11) pp. 2897-2905.

[40] Pereira, F., Lu, J., Castano-Graff, E., 2007, "Microscale 3D Flow Mapping with Mu DDPIV," Experiments in Fluids, **42**(4) pp. 589-599.

[41] Lu, J., Pereira, F., Fraser, S. E., 2008, "Three-Dimensional Real-Time Imaging of Cardiac Cell Motions in Living Embryos," Journal of Biomedical Optics, **13**(1) pp. 014006.

[42] Tien, W., and Dabiri, D., 2013, "Color-Coded Three-Dimensional Micro Particle Tracking Velocimetry and Its Applications," International Symposium on Applications of Laser Techniques to Fluid Mechanics, Lisbon, Portugal, July9-25, 2012.

[43] Tien, W., Kartes, P., Yamasaki, T., 2008, "A Color-Coded Backlighted Defocusing Digital Particle Image Velocimetry System," Experiments in Fluids, **44**(6) pp. 1015-1026.

[44] Lieu, V. H., House, T. A., and Schwartz, D. T., 2012, "Hydrodynamic Tweezers: Impact of Design Geometry on Flow and Microparticle Trapping," Analytical Chemistry, **84**(4) pp. 1963-1968.

[45] Anderson, J. R., Chiu, D. T., Wu, H., 2000, "Fabrication of Microfluidic Systems in Poly (Dimethylsiloxane)," Electrophoresis, **21**pp. 27-40.

[46] Duffy, D. C., McDonald, J. C., Schueller, O. J., 1998, "Rapid Prototyping of Microfluidic Systems in Poly (Dimethylsiloxane)," Analytical Chemistry, **70**(23) pp. 4974-4984.

[47] Lei, Y., Tien, W., Duncan, J., 2012, "A Vision-Based Hybrid Particle Tracking Velocimetry (PTV) Technique using a Modified Cascade Correlation Peak-Finding Method," Experiments in Fluids, **53**(5) pp. 1251-1268.

[48] Maas, H. G., Gruen, A., and Papantoniou, D., 1993, "Particle Tracking Velocimetry in 3-Dimensional Flows .1. Photogrammetric Determination of Particle Coordinates," Experiments in Fluids, **15**(2) pp. 133-146.

[49] Alex, C., 2006, "Scattered Data Interpolation and Approximation using Radial Base Functions," **2009**(April) .

[50] Scott, G. L., and Longuethiggins, H. C., 1991, "An Algorithm for Associating the Features of 2 Images," Proceedings of the Royal Society of London Series B-Biological Sciences, **244**(1309) pp. 21-26.

[51] Duncan, J., Dabiri, D., Hove, J., 2010, "Universal Outlier Detection for Particle Image Velocimetry (PIV) and Particle Tracking Velocimetry (PTV) Data," Measurement Science & Technology, **21**(5) pp. 057002.

[52] Pereira, F., and Gharib, M., 2002, "Defocusing Digital Particle Image Velocimetry and the Three-Dimensional Characterization of Two-Phase Flows," Measurement Science & Technology, **13**(5) pp. 683-694.